bioRxiv preprint doi: https://doi.org/10.1101/145912; this version posted June 4, 2017. The copyright holder for this preprint (which was not certified by peer review) is the author/funder. All rights reserved. No reuse allowed without permission.

Molecular Recognition of Dopamine with Dual Near Infrared Excitation-Emission Two-Photon Microscopy

Jackson Travis Del Bonis-O'Donnell,[1] Ralph H. Page,[1] Abraham G. Beyene,[1] Eric G. Tindall,[1] Ian R. McFarlane,[1] Markita P. Landry [1,2,3]*

[1] Chemical and Biomolecular Engineering, University of California, Berkeley, CA

[2] California Institute for Quantitative Biosciences, QB3, University of California, Berkeley, CA

[3] Chan-Zuckerberg Biohub, San Francisco, CA

To whom correspondence should be addressed: *landry@berkeley.edu

A key limitation for achieving deep imaging in biological structures lies in photon attenuation of fluorescence. In particular, neurotransmitter imaging is challenging in the biologically-relevant context of the intact brain, for which photons must traverse the cranium, skin, and bone. Thus, fluorescence imaging is limited to the surface cortical layers of the brain, only achievable with a craniotomy. Herein, we describe optimal excitation and emission wavelengths for through-cranium imaging, and demonstrate that near-infrared emissive nanosensors can be photoexcited using a two-photon 1550 nm excitation source. Dopamine-sensitive nanosensors can undergo 2-photon excitation, and provide chirality-dependent responses selective for dopamine with fluorescent turn-on responses varying between 20% and 350%. We further calculate the 2-photon absorption cross-section and quantum yield of dopamine nanosensors, and confirm a 2-photon power law relationship for the nanosensor excitation process. Finally, we show improved image quality of nanosensors imbedded 2 mm deep into a brain-mimetic tissue phantom, whereby 1-photon excitation yields 42% scattering, in contrast to 4% scattering when the same object is imaged under 2-photon excitation. Our approach overcomes traditional limitations in deep-tissue fluorescence microscopy, and can enable neurotransmitter imaging in the biologically-relevant milieu of the intact and living brain.

bioRxiv preprint doi: https://doi.org/10.1101/145912; this version posted June 4, 2017. The copyright holder for this preprint (which was not certified by peer review) is the author/funder. All rights reserved. No reuse allowed without permission.

Despite progress towards understanding brain function at a molecular and cellular level, insight into the detailed operation of brain circuits at an emergent level remains elusive.[1] In particular, the development of optical sensors capable of monitoring *in vivo* neurotransmission with high spatial and temporal resolution can enable neuroscientists to broadly monitor the behavior of neuronal cells throughout neural circuits. Recently, semiconducting single-walled carbon nanotubes (SWNTs), which consist of a monolayer of graphene rolled into a cylinder with nanometer diameters and high aspect ratio, have emerged as an engineered nanomaterial readily adaptable for use in neuroscience and general bioimaging.[2, 3] The suitability of SWNTs to these applications arises from their small size (~10^{-9} m diameter, ~10^{-6} m length) and their inherent fluorescence that falls within the near infrared window (NIR-I, 700-900 nm; NIR-II, 1000-1700 nm), coinciding with local minima in the absorbance and scattering spectra of water, blood and brain tissue, respectively.[4-7] *In vivo* deep tissue imaging could be accomplished in the near infrared optical regime, in particular for transcranial detection of modulatory neurotransmitters whose biologically-relevant milieu is in the intact brain of awake and behaving animals. Recently, SWNT suspensions have been demonstrated as contrast agents for transcranial imaging of the mouse vasculature without the need for a cranial imaging window.[8, 9] In parallel, the utility of SWNT fluorophores was expanded beyond their use as a fluorescence contrast agent by functionalizing them with bio-mimetic polymers to recognize biological analytes – thus translating their use as biosensors.[10] To date, these fluorescent nanosensors have been used to detect a variety of biomolecules including dopamine, fibrinogen, nitric oxide, riboflavin and estradiol, to name a few.[10-13] These *in vitro* nanosensors will likely engender real-time *in vivo* neuroscience imaging applications exploiting the biocompatibility, NIR emission, and remarkable photostability of functionalized SWNTs.

One major factor limiting fluorescence brain imaging has been signal attenuation from absorption and scattering excitation photons. To mitigate these obstacles, neuroscientists and biologists have long relied on two-photon microscopy (2PM) using deep-penetrating, NIR light for the non-linear excitation of fluorophores.[14-16] In neuroscience, 2PM has been employed to image strongly scattering brain tissue to study synaptic plasticity in cortical circuits,[17] and to image the dynamics of Na^+ and Ca^{2+} in intact central neurons in their native environment.[18, 19] The benefits of non-linear excitation imaging are also exploited in orthogonal fields of study, including tumorigenesis,[20] embryogenesis[21] and immunology.[16, 22] However, the photons emitted by two-photon excitation (2PE) are subject to the same

bioRxiv preprint doi: https://doi.org/10.1101/145912; this version posted June 4, 2017. The copyright holder for this preprint (which was not certified by peer review) is the author/funder. All rights reserved. No reuse allowed without permission.

absorption and scattering as those that emanate from one-photon excitation (1PE). Absorption and scattering of the signal from visible-wavelength photons emitted by fluorophores limit imaging depth[23] and motivate the use of far-red and NIR fluorophores in brain imaging.[24-26]

The need for robust NIR fluorophores multiphoton imaging, and a parallel interest in SWNTs for imaging and sensing applications, warrants an examination of nonlinear SWNT fluorescence for imaging. Multiphoton fluorescence imaging using NIR light has been demonstrated for a variety of different nanomaterials for biological imaging, but all suffer from the same drawback as many classical fluorophores: emission is confined to the visible or NIR-1 windows.[27-30] In contrast, non-linear excitation of SWNT nanosensors has the advantages of excitation *and* fluorescence emission in the NIR-II window,[31] making them particularly well suited for imaging and sensing in brain tissue. Although SWNTs can be polymer-functionalized for use as real-time neurotransmitter nanosensors for potential *in vivo* imaging,[11] little work has been done to explore NIR 2PE of these functionalized SWNT nanosensors.

Here, we show that 2PE of both DNA-wrapped multi-chirality SWNTs, and surfactant dispersed single-chirality SWNTs, is achievable with a 1560 nm femtosecond pulsed erbium laser. We compute the quantum yield and the two-photon absorption cross-section using (6,5) chirality SWNTs suspended in a sodium dodecyl sulfate, (SDS) using a reference dye, 3,3′-diethylthiatricarbocyanine perchlorate (DTTC), whose quantum yield and two-photon cross section are known.[32] Furthermore, we demonstrate molecular recognition of dopamine using our nanosensors and 2PE, achieving a two-fold increase in SWNT nanosensor fluorescence in the presence of 100 μM dopamine. Our results confirm that the molecular recognition principle is unaltered by the method of photoexcitation (1PE vs. 2PE), and provide a quantitative estimate of SWNT 2PE absorption cross section and quantum yield. Lastly, we show that 2PE yields significantly improved fluorescence spatial resolution over 1PE when SWNT are imaged 2 mm-deep in a strongly scattering intralipid tissue phantom, motivating future *in vivo* applications in 2PM of nanosensors with near infrared fluorescence, henceforth referred to as dual NIR excitation-emission (NIR-EE) microscopy.

bioRxiv preprint doi: https://doi.org/10.1101/145912; this version posted June 4, 2017. The copyright holder for this preprint (which was not certified by peer review) is the author/funder. All rights reserved. No reuse allowed without permission.

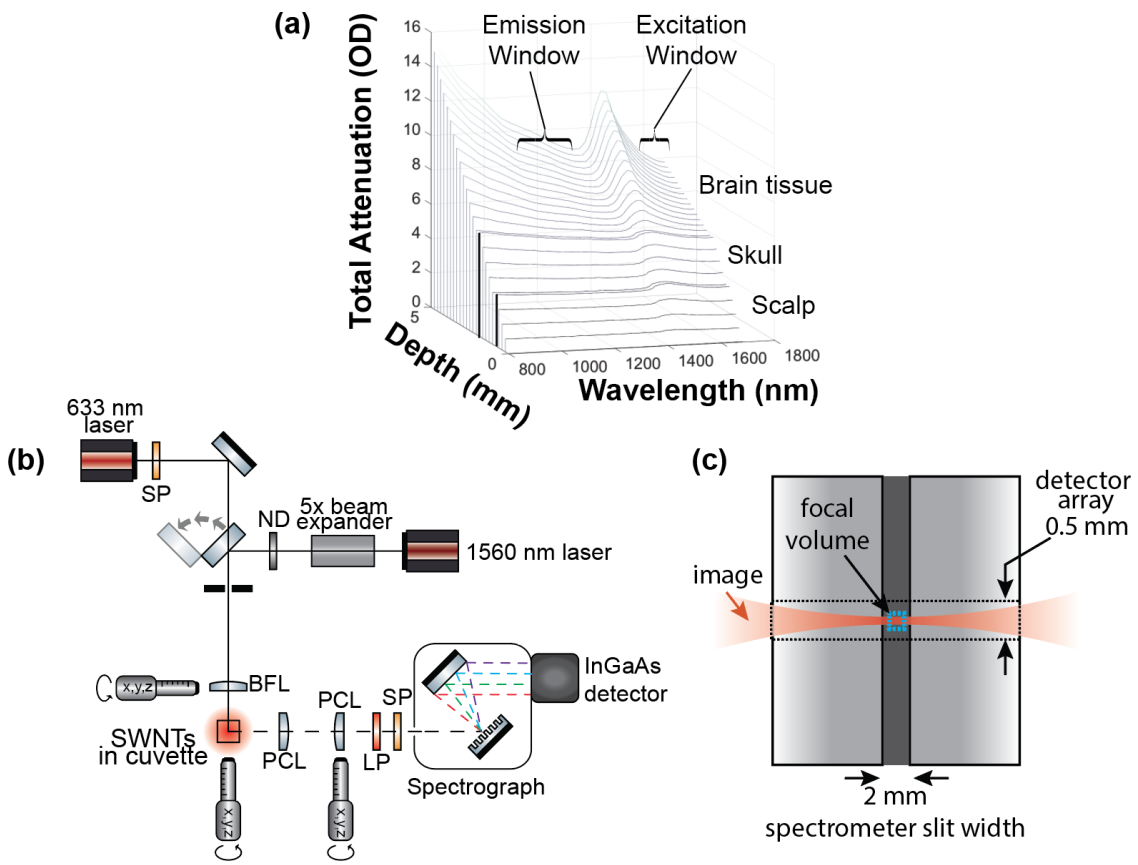

Figure 1. NIR-EE fluorescence microscopy for imaging in highly scattering media. (a) Total photon attenuation (absorbance and scattering) for 1 mm layers of scalp and skull as a function of imaging depth into mouse brain tissue. Both emission and 2-photon excitation of SWNTs fall within local attenuation minima. (b) Schematic depicting collection of fluorescence emission spectra from SWNT samples using the 633 nm laser for 1PE and 1560 nm laser for 2PE. BFL: best-form lens, PCL: planoconvex lens, SP: shortpass filter, LP: longpass filter. Light path terminates into a spectrometer with an InGaAs detector. (c) Magnified diagram showing the focal volume of the laser in the cuvette relative to the spectrometer slit and detector array height.

Motivated by the potential to use NIR SWNT neurotransmitter nanosensors for deep-tissue imaging, we first consider the relationship between imaging wavelength, imaging depth, and fluorescence attenuation, to identify excitation and emission wavelengths of local attenuation minima. Our total photon attenuation calculation takes into account literature values for the absorbance of scalp skin (1 mm), cranial bone (1 mm), and water, in addition to the scattering of scalp skin, cranial bone and brain tissue.[8] Figure 1a shows that SWNT NIR emission coincides with a local attenuation minimum in the 1000-1400 nm range, prior to a local water absorption peak at 1400 nm. Figure 1a also shows a second attenuation minimum in the

bioRxiv preprint doi: https://doi.org/10.1101/145912; this version posted June 4, 2017. The copyright holder for this preprint (which was not certified by peer review) is the author/funder. All rights reserved. No reuse allowed without permission.

1600-1800 nm, which we identify as the optimal 2PE window. Thus, to evaluate SWNTs as NIR fluorophores for two-photon microscopy, we compared fluorescence emission spectra of aqueous solutions of well-dispersed SWNTs using 1PE and 2PE. Using a HeNe laser (633 nm) as a 1PE source, and a femtosecond erbium laser (1560 nm, near the second attenuation minimum) as a 2PE source, we collected emission spectra for two dispersed SWNT samples, i) A dopamine responsive nanosensor composed of HiPco SWNTs wrapped with the single stranded DNA sequence $(GT)_{15}$ and ii) SWNTs suspended in SDS and enriched to contain primarily (6,5) chirality SWNTs. The 2PE source wavelength (1560 nm) is sufficiently far from the linear absorbance of SWNTs (500-900 nm), ensuring that any fluorescence emission observed is on account of non-linear absorption processes. For both 1PE and 2PE, we employed a perpendicular-geometry fluorescence excitation/detection setup (Figure 1b) with a quartz cuvette mounted on a pair of translation stages that enabled accurate placement of the fluorophore sample with respect to the pump-beam waist. The pump light was focused into the cuvette containing SWNT or a reference dye, (DTTC), with a waist radius of 5 μm and a confocal distance of 100 μm in free space. Fluorescence emission from the focal volume was collected at 90 degrees and imaged onto a Princeton Instruments SCT 320 spectrometer with a liquid nitrogen cooled InGaAs array (Figure 1b). Details of the optical setup are outlined in the Supporting Information.

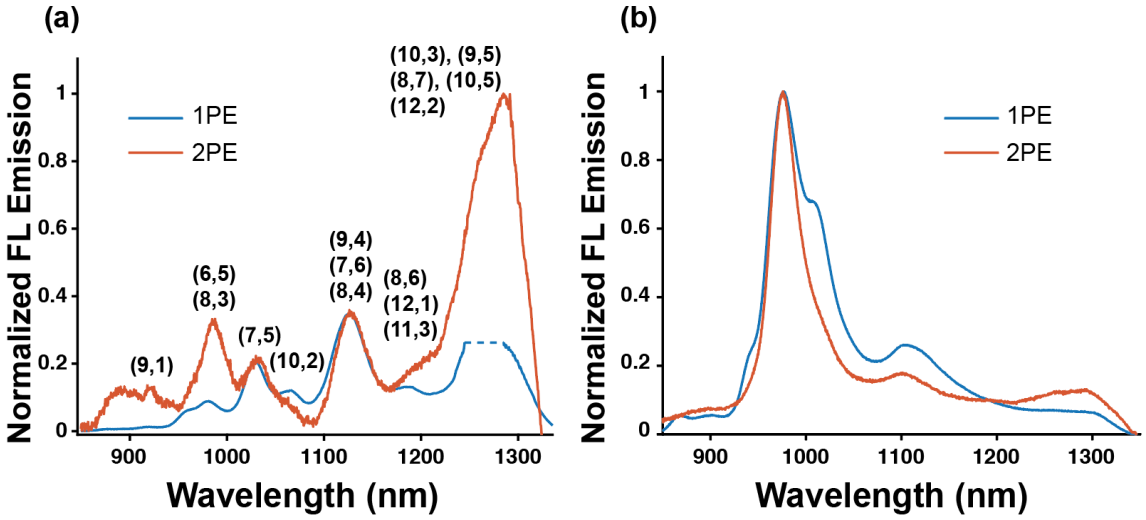

Figure 2. 1PE and 2PE emission spectra of SWNT. Fluorescence emission of (a) $(GT)_{15}$DNA-SWNT and (b) SDS-(6,5)-chirality SWNT suspensions excited with a 633 nm CW 1 photon excitation source (blue) or a 1550 nm fs-pulsed 2 photon excitation source (orange). Labels indicate the chiralities that contribute to each peak. Note: dotted line indicates region of saturated nanosensor fluorescence caused by 2nd order scattered laser light.

bioRxiv preprint doi: https://doi.org/10.1101/145912; this version posted June 4, 2017. The copyright holder for this preprint (which was not certified by peer review) is the author/funder. All rights reserved. No reuse allowed without permission.

As expected, the fluorescence emission spectra of multi-chirality $(GT)_{15}$DNA-wrapped SWNT dopamine nanosensors using 1PE contains multiple peaks in the NIR-II range corresponding to the convolution of emissions from a mixture of different SWNT chiralities (Figure 2a).[33] We deconvolve the contributions of each SWNT chirality to emission peaks using a non-linear least squares method (See Supporting Information Figures S1 & S2, Tables S1 & S2).[10] The prominent emission peaks at 1030 nm and 1126 nm are consistent with on-resonance excitation of (7,5) and (7,6) chirality SWNTs, respectively, in addition to contributions from other chiralities excited off-resonance. The emission peak at 1265 nm is a convolution of (10,3), (9,5) and (11,1) chirality SWNTs excited on-resonance, along with off-resonance SWNTs. Emission peaks from additional SWNT chiralities excited off-resonance are also visible.

Using 2PE, we observed comparable fluorescence emission from $(GT)_{15}$DNA-SWNT nanosensors to establish that SWNT-based dopamine nanosensors are amenable to multi-photon excitation in aqueous solution (Figure 2a). As expected, the 2PE emission spectrum of the DNA-wrapped SWNTs reveals a change in the chiralities excited on-resonance when compared to the 1PE emission spectrum. Normalizing both 1PE and 2PE emission spectrum to the 1126 nm peak (dominant peak for 1PE) shows a three-fold increase in relative emission intensity of (6,5) chirality SWNT, indicating an increase in excitation efficiency. This is consistent with previous measurements of the 2PE emission for (6,5) chirality SWNT which show on-resonance excitation near 1560 nm for dried or surfactant suspended samples.[31, 34] A similar increase in excitation efficiency is observed for chiralities emitting above 1200 nm, which has not been previously reported. This increase likely arises from on-resonance 2PE excitation of (10,3) and (11,1) chiralities, which share 1PE emission peaks closer to that of (6,5) SWNTs.

To further characterize 2PE emission of SWNTs, we prepared a sample enriched with (6,5) chirality dispersed SWNTs through previously reported protocols.[35] Briefly, HiPco SWNT dispersed in SDS by probe tip sonication were purified by adsorption column chromatography through separation over a series of sephacryl gel beds. Through this process, we obtain a chirality purified fraction of enriched (6,5) SWNT, while eliminating SWNT bundles, aggregates and non-emissive metallic SWNTs. Absorbance spectrum measurements of the purified sample (Supporting Information Fig. S2a) reveal prominent peaks associated with the E_{22} *and* E_{11} transitions of (6,5) chirality SWNTs. The 1PE emission spectrum (Figure 2b) shows emission peaked at 975 nm, corresponding to (6,5) chirality

bioRxiv preprint doi: https://doi.org/10.1101/145912; this version posted June 4, 2017. The copyright holder for this preprint (which was not certified by peer review) is the author/funder. All rights reserved. No reuse allowed without permission.

SWNTs, with additional fluorescence peaks near 1000 nm and 1100 nm resulting from other SWNT chiralities remaining after purification. The relative emission intensity of these off-resonance chiralities, however, is minimal. 2PE excitation of the (6,5) chirality was tested by changing the laser excitation source from a 633 nm CW to a 1560 nm fs-pulsed erbium laser. 2PE emission spectra from (6,5) SWNT show a dominant emission peak at 975 nm (Figure 2b), as with 1PE excitation. Furthermore, the fluorescent contribution of non-(6,5) chiralities decreases in the spectrum collected using 2PE compared to 1PE due to off-resonance excitation, consistent with our observations of the mixed-chirality SWNT sample.

Emission intensity of the (6,5) chirality SWNTs increased without a change in the emission lineshape as the 2PE laser power was varied from 3 mW to 70mW (Figure 3). The integrated emission intensity as a function of laser power exhibited a quadratic dependence as indicated by a slope of nearly 2 for the linear fit to the log-log plot of SWNT fluorescence intensity versus laser excitation power (Figure 3, inset), confirming the SWNT fluorescence resulted from a non-linear photon absorption process.

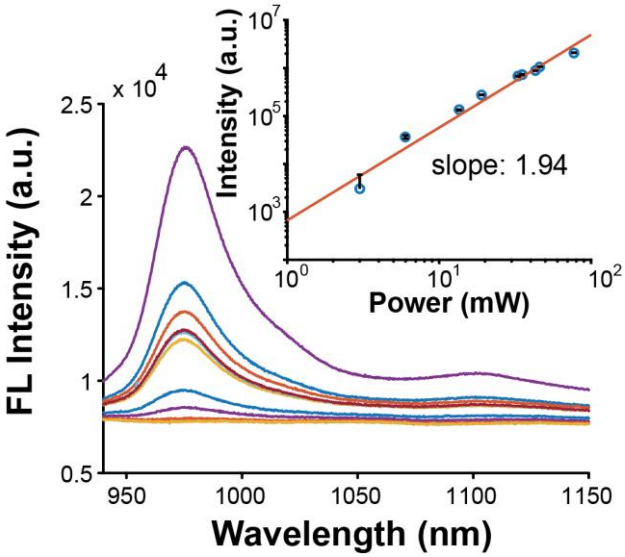

Figure 3. Emission spectra of SDS-(6,5)-enriched SWNTs excited with 2 photon excitation at different laser powers. The integrated emission intensity increases quadratically with laser power as shown by the near 2 slope of a log-log plot of the emission intensity as a function of laser power (inset). A background signal, comprised of the integrated intensity at an incident power below which appreciable changes in signal were observed, was subtracted prior to integration. The magnitude of error bars (inset) reflects this integrated background signal.

bioRxiv preprint doi: https://doi.org/10.1101/145912; this version posted June 4, 2017. The copyright holder for this preprint (which was not certified by peer review) is the author/funder. All rights reserved. No reuse allowed without permission.

The 1PE quantum yield, Q_{1P}, and absorption cross section for 2PE, σ_{2P}, are useful values for comparing fluorophores for use in 2PM, as the fluorescence signal from 2PE depends linearly on these two values (see Supporting Information for details). Q_{1P}, can be calculated for a sample (S) fluorophore by comparing its behavior to a reference (R) fluorophore with the following equation:[36]

$$Q_{1P,S} = Q_{1P,R}\left(\frac{n_{1P,S}}{n_{1P,R}}\right)^2 \frac{S_{1P,S}}{A_{1P,S}}\frac{A_{1P,R}}{S_{1P,R}} \qquad (1)$$

where S is the number of emission photons detected per unit time, A is the absorbed fraction of the impinging pump light, n is index of refraction and subscripts of S and R represent the sample fluorophore and reference fluorophore respectively. S is measured by the integral:

$$S = \frac{1}{T}\int \frac{I_{raw}(\lambda)}{R(\lambda)} d\lambda \qquad (2)$$

where T is the integration time period, $I_{raw}(\lambda)$ is the raw intensity of detected emission photons, and $R(\lambda)$ is the wavelength-dependent response of the spectrometer and dark-current offsets. With $Q_{1P,S}$ calculated, $\sigma_{2P,S}$ can be computed using a similar comparison:[36]

$$\sigma_{2P,S} = \sigma_{2P,R}\left(\frac{n_{2P,S}}{n_{2P,R}}\right)^2 \frac{S_{2P,S}}{N_{2P,S}Q_{1P,S}}\frac{N_{2P,R}Q_{1P,R}}{S_{2P,R}} \qquad (3)$$

where N is the number density of fluorophores per unit volume. Note that errors in $Q_{1P,S}$ propagate into the $\sigma_{2P,S}$ estimate. It is assumed that pumping is below the onset of saturation for both the 1PE and 2PE systems.

For this work, the sample fluorophore tested was the purified (6,5) SWNT. This was in lieu of a multi-chirality, and thus multi-emitter, suspension of SWNTs to simplify the $Q_{1P,S}$ calculation. The reference fluorophore used was 3,3′-diethylthiatricarbocyanine perchlorate (DTTC), as it is a NIR emitting dye with previously characterized Q_{1P} and σ_{2P}.[32] Absorbance and emission spectra are shown in the Supporting Information (Figures S3, S4 and S5). Calibrations and additional considerations for Q_{1P} and σ_{2P} calculations as well as calibration corrected spectra are outlined in the Supporting Information (Figures S6, S7, S8, S9). Following these methods and calculations we measure $Q_{1P,SWNT} = 0.0023$ and $\sigma_{2P,SWNT} = 239{,}000$ GM. Note that 1 GM, the unit of two-photon absorption cross section, is

bioRxiv preprint doi: https://doi.org/10.1101/145912; this version posted June 4, 2017. The copyright holder for this preprint (which was not certified by peer review) is the author/funder. All rights reserved. No reuse allowed without permission.

defined as 10^{-50} cm^4 sec/photon. Values for $Q_{1P,SWNT}$ reported in literature range from 10^{-4} to a few percent, whereas $\sigma_{2P,SWNT}$ can be inferred from previous work as ranging from 10,000 GM to 700,000 GM.[31, 37-43] Both our $Q_{1P,SWNT}$ and $\sigma_{2P,SWNT}$ fall within ranges expected based on data from these previous reports. A detailed list of input values is included in Tables S3 and S4 of the Supporting Information. Given our experimental conditions, we would expect an imaging resolution of approximately the beam waist, 4.8 μm, to produce an image using pixel dwell times on the order of milliseconds. Micron length and millisecond time frames are in-line with the requisite imaging parameters necessary to capture relevant processes in brain neurotransmission.

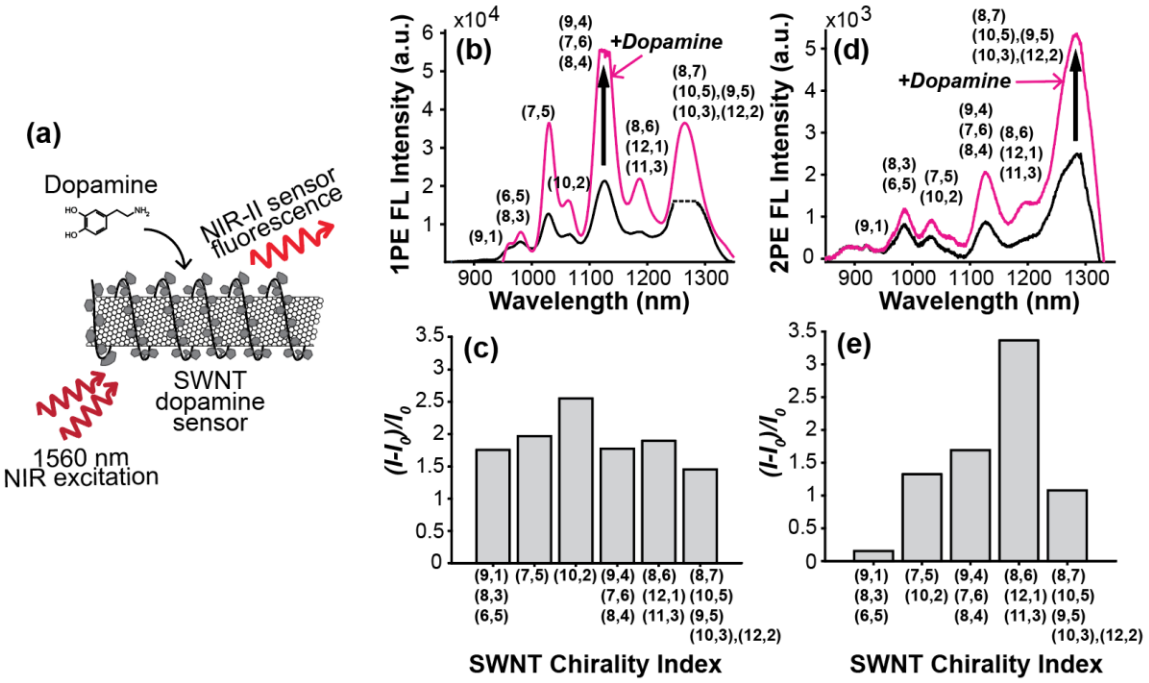

Figure 4. Fluorescence response of dopamine nanosensors using one- and two-photon excitation. (a) Schematic depicting dopamine binding a dopamine nanosensor and the resulting fluorescence emission enhancement. Dopamine (100μM) increases the fluorescence emission intensity of $(GT)_{15}$DNA wrapped SWNTs using both 1PE (b)-(c) and 2PE (d)-(e). Note: dotted line indicates region of saturated nanosensor caused by 2nd order scattered laser light.

Next, we evaluated the efficacy of 2PE for neurotransmitter detection using a dopamine-sensitive SWNT nanosensor. $(GT)_{15}$DNA polymer-functionalized SWNTs are a recently discovered NIR optical nanosensors enabling the selective and reversible sensing of the neuromodulatory neurotransmitter dopamine.[11] These SWNT-based dopamine nanosensors

bioRxiv preprint doi: https://doi.org/10.1101/145912; this version posted June 4, 2017. The copyright holder for this preprint (which was not certified by peer review) is the author/funder. All rights reserved. No reuse allowed without permission.

exhibit a marked increase in fluorescence emission intensity upon binding dopamine with sensitivities down to 10 nM. To date, the fluorescence response of SWNT dopamine nanosensors has only been characterized using one-photon visible wavelength excitation. We aim to determine whether SWNT-based dopamine nanosensors are compatible with NIR-EE microscopy for multi-photon deep-tissue imaging applications, which requires the nanosensor's 'turn-on' fluorescence response to dopamine to be indifferent to the SWNT photon absorption process. Using both 1PE and 2PE, fluorescence emission spectra were collected from a sample of $(GT)_{15}$DNA-SWNT dopamine nanosensors before and after the addition of 100 μM dopamine (Figure 3). Adding dopamine increases the fluorescence emission intensity for all SWNT chiralities for both 1PE and 2PE, confirming that the response is independent of the photon absorption process. We calculated the relative change in peak fluorescence intensity for different SWNT chiralities by first deconvolving the SWNT emission spectra (see Supporting Information) and calculating the dopamine nanosensor signal, $(I\text{-}I_0)/I_0$, where I_0 is the integrated fluorescence intensity for each SWNT chirality before dopamine addition. We combined the integrated intensities into groups of chiralities that had indistinguishable emission spectra, e.g. the integrated emission of (9,1), (8,3), and (6,5) were combined into a single group. For both excitation methods, the fluorescence intensity of SWNT nanosensors increases with the addition of dopamine for all SWNT chiralities. For 1PE, the response is only mildly dependent on chirality and varies between 145% and 255%, comparable to previous measurements.[11, 44] The fluorescence response using 2PE shows considerably more chirality dependence, with maximal dopamine-induced fluorescence increases observed for longer NIR-II wavelengths (1100 nm – 1350 nm). The chirality dependence observed for 2PE is likely due to discrepancies between the excitation efficiencies of different chirality SWNTs using NIR compared to visible light. The benefit of 2PE excitation of dopamine nanosensors, combined with their enhanced NIR-II emissions above 1100 nm (Figure 1a), motivates their use in highly scattering biological media and for deep-tissue imaging using 2PM for NIR-EE microscopy.

bioRxiv preprint doi: https://doi.org/10.1101/145912; this version posted June 4, 2017. The copyright holder for this preprint (which was not certified by peer review) is the author/funder. All rights reserved. No reuse allowed without permission.

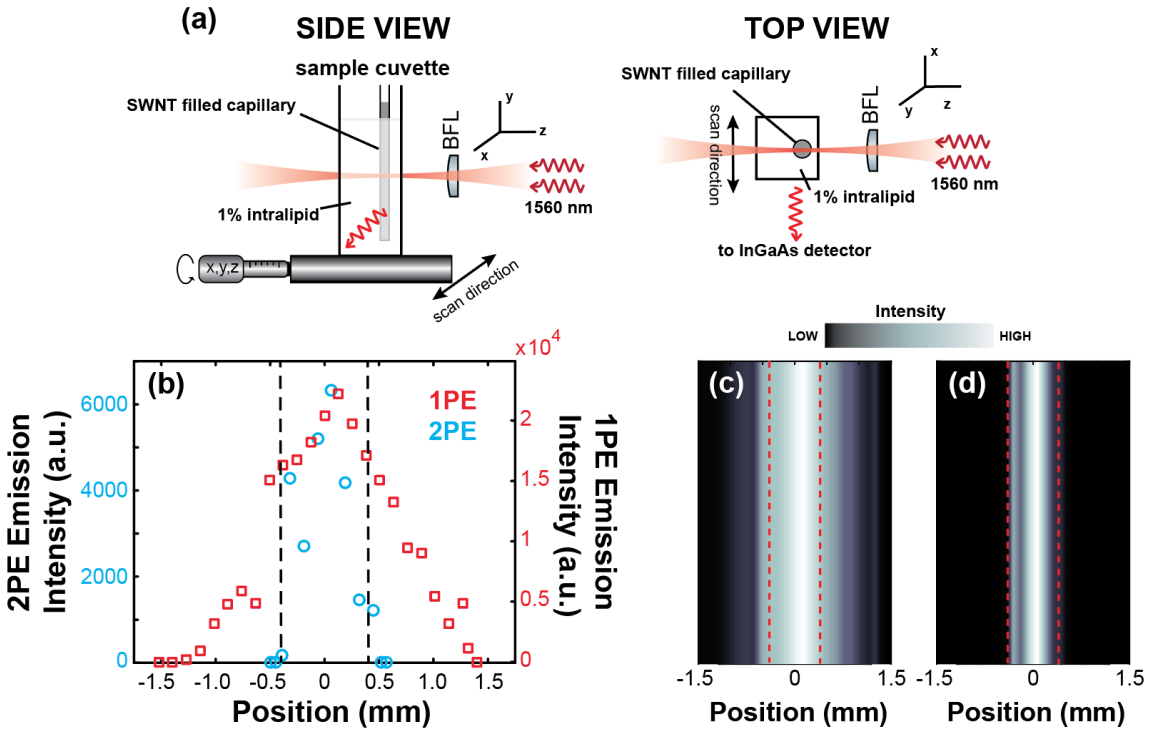

Figure 5. Improved spatial resolution at 2 mm Intralipid imaging depth with NIR-EE microscopy. (a) Schematic depicting a SWNT-filled 0.8 mm- inner diameter capillary submerged in a strongly scattering solution (1% Intralipid) at a depth of 0.5 mm from the excitation edge of the cuvette and at an Intralipid depth of 2 mm from the cuvette emission edge. The sample cuvette and capillary were scanned in the x-direction through the beam focus. (b) Integrated fluorescence intensity as a function of scan position as the capillary is scanned across the focused beam using 1PE (red squares) and 2PE (blue circles). For reference, the dashed black lines indicate the position of the capillary edge. The intensity data presented in (b) is reconstructed into one-dimensional line scan images for (c) 1PE and (d) 2PE with dashed red line indicating the position of the capillary edge.

To demonstrate the advantages of two-photon over one-photon fluorescence imaging of SWNT-based nanosensors, we compared reconstructed images of a SWNT-filled capillary immersed in a highly scattering tissue phantom, 1% Intralipid solution,[6, 8, 23] under 1PE versus 2PE. Of relevance to deep-brain imaging of dopamine, the tissue phantom simulates both the absorbance due to water as well as the scattering brain tissue.[8] An 800 μm inner diameter quartz capillary was filled with a (6,5)-chirality purified SWNT suspension and placed into the cuvette containing 1% Intralipid (see materials and methods) at an Intralipid depth of 0.5 mm from the surface of the cuvette facing the excitation focusing lens (excitation Intralipid depth), and an Intralipid depth of 2 mm from the capillary surface facing the InGaAs

bioRxiv preprint doi: https://doi.org/10.1101/145912; this version posted June 4, 2017. The copyright holder for this preprint (which was not certified by peer review) is the author/funder. All rights reserved. No reuse allowed without permission.

detector (emission Intralipid depth). We reconstruct a 1-dimensional image of the capillary by scanning the capillary laterally across the focused beam using a translation stage and collecting the emitter NIR fluorescence in the transverse direction (Figure 5a). Each pixel of this one-dimensional line scan is generated by the summed detector intensity at each focusing lens position (Figure 5b), and used to reconstruct an image of the capillary (Figure 5c, d). The scattering of 633 nm excitation photons by the Intralipid occluding the intra-capillary SWNTs produces a severely blurred image (Figure 5c) with poorly resolved edges relative to the actual capillary outline. Visible wavelength excitation scattering occurred even when the laser focus was as far as 1 mm from the actual edge of the capillary. In contrast, the image constructed using 2PE via 1560 nm laser excitation resolved sharp edges of the capillary (Figure 5d), allowing for precise image reconstruction of the capillary diameter.

These results demonstrate the advantages of using 2PE for deep-tissue imaging in combination with NIR-I and NIR-II emissive fluorophores, namely reduced scattering of incident excitation photons. Herein, we show that NIR-EE microscopy builds upon the advantages of conventional 2PE by both exciting and collecting photons in local tissue transparency minima (Figure 1a). By minimizing scattering of incident photons, we can enhance localization of excitation to improve imaging quality. For our capillary images, 42% of the integrated collected fluorescence occurred beyond the extant of the physical capillary boundaries using 1PE compared to only 4% scattering-induced image blurring using 2PE. Additionally, bio-mimetic polymer functionalization of SWNT for molecular detection of modulatory neurotransmitters improves the utility beyond the use of SWNT as biological contrast imaging agents, and demonstrate their inherent advantages for detection of biological targets in strongly scattering tissues. In particular, NIR-EE imaging of SWNT-based modulatory neurotransmitter nanosensors could enable real-time fluorescence monitoring of analytes such as dopamine in optically dense brain tissue.

In summary, we demonstrate NIR-II fluorescence-based imaging of the neurotransmitter dopamine using NIR-II laser excitation of functionalized SWNT nanosensors. To evaluate the efficacy of using 2PE of SWNT nanosensors for imaging applications, we measure the quantum efficiency, Q_{1P}, and absorption cross section of 2PE, σ_{2P}, as 0.0023 and 239,000 GM, respectively. Using the current configuration, these values establish reasonable estimates for laser dwell times on the order of milliseconds for constructing images with resolution of ~5 μm using scanning imaging microscopy. Comparisons of 1PE and 2PE scanning imaging of a NIR SWNT-filled capillary in turbid intralipid tissue phantoms confirm that the reduced

bioRxiv preprint doi: https://doi.org/10.1101/145912; this version posted June 4, 2017. The copyright holder for this preprint (which was not certified by peer review) is the author/funder. All rights reserved. No reuse allowed without permission.

scattering of NIR-II incident excitation light improves fluorescence spatial resolution and imaging quality as shown by sharper image boundaries and better localization of integrated SWNT NIR fluorescence. Our results inspire the use of NIR SWNT nanosensors and 2PE in future investigations involving real-time imaging of dopamine directly in the highly-scattering tissue of the brain.

Corresponding Author

*Email: landry@berkeley.edu

ORCID

Jackson Travis Del Bonis-O'Donnell: 0000-0002-9135-2102

Markita Landry: 0000-0002-5832-8522

Author Contributions

The manuscript was written through contributions of all authors. M.P.L. and J.T.D.O. conceived the concept of Dual NIR Excitation-Emission microscopy. All authors contributed to experimental design, data acquisition, analysis, and calculations. All authors have approved the final version of the manuscript.

Notes

The authors declare no competing financial interest.

ACKNOWLEDGMENTS

Our work was supported by a Burroughs Wellcome Fund Career Award at the Scientific Interface (CASI), the Simons Foundation, a BBRF young investigator award, and a Beckman Foundation Young Investigator Award (M.P.L.). M.P.L. is a Chan Zuckerberg Biohub investigator. A.B. Acknowledges the support of an NSF Graduate Research Fellowship.

bioRxiv preprint doi: https://doi.org/10.1101/145912; this version posted June 4, 2017. The copyright holder for this preprint (which was not certified by peer review) is the author/funder. All rights reserved. No reuse allowed without permission.

REFERENCES

1. Alivisatos, A. P.; Andrews, A. M.; Boyden, E. S.; Chun, M.; Church, G. M.; Deisseroth, K.; Donoghue, J. P.; Fraser, S. E.; Lippincott-Schwartz, J.; Looger, L. L.; Masmanidis, S.; McEuen, P. L.; Nurmikko, A. V.; Park, H.; Peterka, D. S.; Reid, C.; Roukes, M. L.; Scherer, A.; Schnitzer, M.; Sejnowski, T. J.; Shepard, K. L.; Tsao, D.; Turrigiano, G.; Weiss, P. S.; Xu, C.; Yuste, R.; Zhuang, X. W. *ACS Nano* **2013,** 7, (3), 1850-1866.

2. Hong, G.; Antaris, A. L.; Dai, H. *Nat. Biomed. Eng.* **2017,** 1, 0010.

3. Roxbury, D.; Jena, P. V.; Williams, R. M.; Enyedi, B.; Niethammer, P.; Marcet, S.; Verhaegen, M.; Blais-Ouellette, S.; Heller, D. A. *Sci. Rep.* **2015,** 5, (August), 14167-14167.

4. Nakane, Y.; Tsukasaki, Y.; Sakata, T.; Yasuda, H.; Jin, T. *Chem. Commun.* **2013,** 49, (69), 7584-7586.

5. Tsukasaki, Y.; Morimatsu, M.; Nishimura, G.; Sakata, T.; Yasuda, H.; Komatsuzaki, A.; Watanabe, T.; Jin, T. *RSC Advances* **2014,** 4, (77), 41164-41171.

6. Welsher, K.; Sherlock, S. P.; Dai, H. *Proc. Natl. Acad. Sci. U.S.A.* **2011,** 108, (22), 8943-8.

7. Movia, D.; Canto, E. D.; Giordani, S. *J. Phys. Chem. C* **2010,** 114, (43), 18407-18413.

8. Hong, G.; Diao, S.; Chang, J.; Antaris, A.; Chen, C.; Zhang, B.; Zhao, S.; Atochin, D.; Huang, P.; Andreasson, K.; Kuo, C.; Dai, H. *Nat. Photon.* **2014,** 8, (9), 723-730.

9. Heller, D. A.; Baik, S.; Eurell, T. E.; Strano, M. S. *Adv. Mater.* **2005,** 17, (23), 2793-2799.

10. Zhang, J.; Landry, M. P.; Barone, P. W.; Kim, J.-H.; Lin, S.; Ulissi, Z. W.; Lin, D.; Mu, B.; Boghossian, A. A.; Hilmer, A. J.; Rwei, A.; Hinckley, A. C.; Kruss, S.; Shandell, M. A.; Nair, N.; Blake, S.; Şen, F.; Şen, S.; Croy, R. G.; Li, D.; Yum, K.; Ahn, J.-H.; Jin, H.; Heller, D. A.; Essigmann, J. M.; Blankschtein, D.; Strano, M. S. *Nat. Nanotechnol.* **2013,** 8, (12), 959-68.

11. Kruss, S.; Landry, M. P.; Vander Ende, E.; Lima, B. M. a.; Reuel, N. F.; Zhang, J.; Nelson, J.; Mu, B.; Hilmer, A.; Strano, M. *J. Am. Chem. Soc.* **2014,** 136, (2), 713-724.

12. Bisker, G.; Dong, J.; Park, H. D.; Iverson, N. M.; Ahn, J.; Nelson, J. T.; Landry, M. P.; Kruss, S.; Strano, M. S. *Nat. Commun.* **2016,** 7, 10241-10241.

bioRxiv preprint doi: https://doi.org/10.1101/145912; this version posted June 4, 2017. The copyright holder for this preprint (which was not certified by peer review) is the author/funder. All rights reserved. No reuse allowed without permission.

13. Kim, J.-H.; Heller, D. A.; Jin, H.; Barone, P. W.; Song, C.; Zhang, J.; Trudel, L. J.; Wogan, G. N.; Tannenbaum, S. R.; Strano, M. S. *Nat. Chem.* **2009,** 1, (6), 473-481.

14. Helmchen, F.; Denk, W. *Nat. Methods* **2005,** 2, (12), 932-940.

15. Williams, R. M.; Zipfel, W. R.; Webb, W. W. *Curr. Opin. Chem. Biol.* **2001,** 5, (5), 603-608.

16. Zipfel, W. R.; Williams, R. M.; Webb, W. W. *Nat. Biotechnol.* **2003,** 21, (11), 1369-1377.

17. Holtmaat, A.; Bonhoeffer, T.; Chow, D.; Chuckowree, J.; De Paola, V.; Hofer, S.; Hubener, M.; Keck, T.; Knott, G.; Lee, W.; Mostany, R.; Mrsic-Flogel, T.; Nedivi, E.; Portera-Cailliau, C.; Svoboda, K.; Trachtenberg, J.; Wilbrecht, L. *Nat. Protoc.* **2009,** 4, (8), 1128-1144.

18. Rose, C.; Kovalchuk, Y.; Eilers, J.; Konnerth, A. *Pflugers Arch., EJP* **1999,** 439, (1-2), 201-207.

19. Nguyen, Q. T.; Callamaras, N.; Hsieh, C.; Parker, I. *Cell Calcium* **2001,** 30, (6), 383-393.

20. Brown, E.; Campbell, R.; Tsuzuki, Y.; Xu, L.; Carmeliet, P.; Fukumura, D.; Jain, R. *Nat. Med.* **2001,** 7, (7), 864-868.

21. Squirrell, J.; Wokosin, D.; White, J.; Bavister, B. *Nat. Biotechnol.* **1999,** 17, (8), 763-767.

22. Cahalan, M.; Parker, I.; Wei, S.; Miller, M. *Nat. Rev. Immunol.* **2002,** 2, (11), 872-880.

23. Dunn, A. K.; Wallace, V. P.; Coleno, M.; Berns, M. W.; Tromberg, B. J. *Appl. Opt.* **2000,** 39, (7), 1194-1201.

24. Horton, N.; Wang, K.; Kobat, D.; Clark, C.; Wise, F.; Schaffer, C.; Xu, C. *Nat. Photon.* **2013,** 7, (3), 205-209.

25. Grutzendler, J.; Kasthuri, N.; Gan, W. *Nature* **2002,** 420, (6917), 812-816.

26. Escobedo, J.; Rusin, O.; Lim, S.; Strongin, R. *Curr. Opin. Chem. Biol.* **2010,** 14, (1), 64-70.

bioRxiv preprint doi: https://doi.org/10.1101/145912; this version posted June 4, 2017. The copyright holder for this preprint (which was not certified by peer review) is the author/funder. All rights reserved. No reuse allowed without permission.

27. Levy, E.; Tajon, C.; Bischof, T.; Iafrati, P.; Fernandez-Bravo, A.; Garfield, D.; Chamanzar, M.; Maharbiz, M.; Sohal, V.; Schuck, P.; Cohen, B.; Chan, E. *ACS Nano* **2016,** 10, (9), 8423-8433.

28. Rubio, N.; Hirvonen, L.; Chong, E.; Wang, J.; Bourgognon, M.; Kafa, H.; Hassan, H.; Al-Jamal, W.; McCarthy, D.; Hogstrand, C.; Festy, F.; Al-Jamal, K. *Chem. Commun.* **2015,** 51, (45), 9366-9369.

29. Feng, X.; Li, Z.; Li, X.; Liu, Y. *Sci. Rep.* **2016,** 6.

30. Larson, D.; Zipfel, W.; Williams, R.; Clark, S.; Bruchez, M.; Wise, F.; Webb, W. *Science* **2003,** 300, (5624), 1434-1436.

31. Wang, F.; Dukovic, G.; Brus, L. E.; Heinz, T. F. *Science* **2005,** 308, (5723), 838-840.

32. Berezin, M. Y.; Zhan, C.; Lee, H.; Joo, C.; Akers, W. J.; Yazdanfar, S.; Achilefu, S. *J. Phys. Chem B* **2011,** 115, (39), 11530-11535.

33. Bachilo, S. M.; Strano, M. S.; Kittrell, C.; Hauge, R. H.; Smalley, R. E.; Weisman, R. B. *Science* **2002,** 298, (5602), 2361-2366.

34. Maultzsch, J.; Pomraenke, R.; Reich, S.; Chang, E.; Prezzi, D.; Ruini, A.; Molinari, E.; Strano, M. S.; Thomsen, C.; Lienau, C. *Phys. Rev. B* **2005,** 72, (24), 241402-241402.

35. Jain, R. M.; Ben-Naim, M.; Landry, M. P.; Strano, M. S. *J. Phys. Chem. C* **2015,** 119, (39), 22737-22745.

36. Xu, C.; Webb, W. W., Multiphoton excitation of molecular fluorophores and nonlinear laser microscopy. In *Top. Fluoresc. Spectrosc.*, Springer: 2002; pp 471-540.

37. Pomraenke, R.; Maultzsch, J.; Reich, S.; Chang, E.; Prezzi, D.; Ruini, A.; Molinari, E.; Strano, M. S.; Thomsen, C.; Lienau, C. *physica status solidi (b)* **2006,** 243, (10), 2428-2435.

38. Wang, F.; Dukovic, G.; Brus, L. E.; Heinz, T. F. *Phys. Rev. Lett.* **2004,** 92, (17), 177401.

39. Cherukuri, T. K.; Tsyboulski, D. A.; Weisman, R. B. *ACS Nano* **2012,** 6, (1), 843-850.

40. Hertel, T.; Himmelein, S.; Ackermann, T.; Stich, D. *ACS Nano* **2010,** 12, (4), 7161-7168.

41. Lisa J. Carlson; Sara E. Maccagnano; Ming Zheng; John Silcox; Todd D. Krauss. *Nano Lett.* **2007,** 12, (7), 3698-3703.

bioRxiv preprint doi: https://doi.org/10.1101/145912; this version posted June 4, 2017. The copyright holder for this preprint (which was not certified by peer review) is the author/funder. All rights reserved. No reuse allowed without permission.

42. Lefebvre, J.; Austing, D. G.; Bond, J.; Finnie, P. *Nano Lett.* **2006,** 6, (8), 1603–1608.

43. Crochet, J.; Clemens, M.; Hertel, T. *J. Am. Chem. Soc.* **2007,** 129, (26), 8058-8059.

44. Salem, D. P.; Landry, M. P.; Bisker, G.; Ahn, J.; Kruss, S.; Strano, M. S. *Carbon* **2016,** 97, 147-153.